Progress In Electromagnetics Research, Vol. 144, 123–132, 2014

Design of Polarization and Incident Angle Insensitive Dual-Band Metamaterial Absorber Based on Isotropic Resonator

Furkan Dincer[1], Muharrem Karaaslan[1], Emin Unal[1], Kemal Delihacioglu[2], and Cumali Sabah[3, *]

Abstract—Polarization and incident angle independent metamaterial-based absorber (MA) which acts as a strong dual-band resonator is designed and constructed. Besides, a method to design single/dual-band MA is presented in detail. The proposed model is based on isotropic ring resonator with gaps and octa-star strip (OSS) which allows maximization in the absorption because of the characteristic features of the structure. Reflection and absorption responses are obtained both numerically and experimentally and compared to each other. Two maxima in the absorption are experimentally obtained around 90% at 4.42 GHz for the first band and 99.7% at 5.62 GHz for the second band which are in good agreement with the numerical simulations (95.6% and 99.9%, respectively). The numerical studies verify that the dual-band MA can provide perfect absorption at wide angles of incidence for both transverse electric (TE) and transverse magnetic (TM) waves. The proposed model can easily be used in many potential application areas such as security systems, sensors, medical imaging technology.

1. INTRODUCTION

MTMs have gained a great deal of interest in the science community due to their unconventional electric and magnetic features. They display specific electromagnetic properties not commonly found in nature and different from conventional materials such as negative permittivity, negative permeability, negative refraction, and so on [1, 2]. In addition, they have wide potential application areas for instance electromagnetic cloaking [3, 4], super lens [5], sensing [6], absorber [7–16], EM filters [17, 18], high-frequency polarization rotators [19], and so on [20–42]. In general, they are artificial, handmade, and effectively homogeneous electromagnetic (EM) materials that can be fabricated and used for the desired range of EM spectrum, from radio to optical frequencies. Among them, the concept of MA has achieved remarkable progress owing to the development of the MTM implementation technology in absorber and absorber type devices. In fact, there were several significant attempts in the literature for the fabrication and usage of MA for several frequencies. Bilotti et al. [7] designed a resonant microwave MA based on SRR-shaped inclusions. Landy et al. [8] presented MA element with near unity absorbance. Their design consists of electric and magnetic resonators as in the present study. Lee and Lim [9] introduced bandwidth-enhanced microwave absorber using a double resonant MTM. Sun et al. [10] designed an extremely broad frequency band absorber based on destructive interference mechanism with multilayered SRRs. Li et al. [11] presented ultra-thin absorber with different resonant modes. Park et al. [12] numerically and experimentally studied the multi-band MA at microwave frequencies. Wang et al. [13] numerically and experimentally proposed a resonant microwave absorber based on a chiral MTM with SRRs. Zhu et al. [14] proposed a polarization modulation scheme of EM waves through reflection of a tunable MTM reflector/absorber. Zhu et al. [15] studied the design, fabrication,

Received 14 November 2013, Accepted 20 December 2013, Scheduled 13 January 2014

* Corresponding author: Cumali Sabah (sabah@metu.edu.tr).

[1] Department of Electrical and Electronics Engineering, Mustafa Kemal University, Iskenderun, Hatay 31200, Turkey. [2] Department of Electrical and Electronics Engineering, Kilis 7 Aralık University, Kilis, Turkey. [3] Department of Electrical and Electronics Engineering, Middle East Technical University, Northern Cyprus Campus, Kalkanli, Guzelyurt, TRNC/Mersin 10, Turkey.

and measurement of a polarization insensitive microwave absorber based on MTM. Additionally, chiral-MTM-based absorber is studied with high absorption at wide angles of incidence for both transverse electric and transverse magnetic waves [27]. Besides, the science community continues to contribute to literature and technology with such kind of studies since MAs have wide potential application areas to be used in several applications [16–41].

In this study, we construct a new dual-band perfect MA which provides polarization and incident angle independency with an easy fabrication by providing a method about designing single/dual-band MA. The proposed dual-band MA is composed of an isotropic ring resonator with gaps and OSS. The results show that the dual-band MA presents perfect absorption at both frequencies of (95.6%) 4.32 GHz and (99.9%) at 5.73 GHz. The experimental results of the considered structure are in good agreement with the numerical studies.

2. DESIGN, SIMULATION, AND MEASUREMENT

The proposed design consists of a isotropic ring resonator with gaps and OSS structure and metallic layer separated by a dielectric substrate as shown in Fig. 1. FR4 is chosen as dielectric substrate and the metallic pattern and ground layer are modeled as copper sheet with electrical conductivity of 5.8001×10^7 S/m and thickness of 0.036 mm. The thickness, loss tangent, and relative permittivity of FR4 are 1.6 mm, 0.02, and 4.2, correspondingly. The unit cell dimensions of the ring resonator with gaps and OSS are $a = 19.90$ mm, $b = 14$ mm, $c = 1$ mm, and $d = 2$ mm as shown in Fig. 1(a). Also, in Fig. 1(b), the periodic arrangement of the fabricated dual-band MA is given. The overall size of the sample is 15 cm × 15 cm (5 × 5 unit cells).

The simulation of the periodic structure was performed with a commercial full-wave EM solver based on finite integration technique. The periodic boundary conditions with floquet port are used in the simulation. To compare the obtained numerical results (with those of the experimental ones), S-parameters of the fabricated MA are measured by using a vector network analyzer and two horn antennas (to measure reflection and transmission coefficients). Firstly, free space measurement without sample is carried out and this measurement used as the calibration data for the VNA. The sample is then inserted into the experimental measurement setup and S-parameter measurements are performed. Fig. 2 shows the measurement setup with VNA and two horn antennas.

The frequency behavior of absorption can be calculated by $A(\omega) = 1 - R(\omega) - T(\omega)$, where $A(\omega)$, $R(\omega)$, and $T(\omega)$ are the absorption, reflectance, and transmittance, in order. Maximizing $A(\omega)$ comes from the minimizing both the reflection $R(\omega) = |S_{11}|^2$ and transmission $T(\omega) = |S_{21}|^2$ generally at the condition of impedance matching at the resonance frequency. There will be no transmission to be examined throughout the present study as the back side of the sample is blocked off by the continuous metal. Therefore, there is only the reflection required to be investigated which is directly related with S_{11}. Consequently, the absorption can be calculated as $A(\omega) = 1 - R(\omega)$. The perfect absorption can be obtained when the reflection is close to zero which is the main aim of the study. Reflectivity can be reduced to near-zero value when the relative effective permittivity $\varepsilon(\omega)$ and permeability $\mu(\omega)$ have the same/similar value due to the impedance matching with air. It is possible to absorb both the incident electric and magnetic fields tremendously by properly tuning $\varepsilon(\omega)$ and $\mu(\omega)$. They can be manipulated to realize a high absorber [9–18]. At the resonance condition, the effective impedance $Z(\omega)$ can match to the free space impedance $Z(\omega) = Z_0(\omega)$ and therefore, the reflection is minimized [9–18]. With this way, perfect absorption can be achieved.

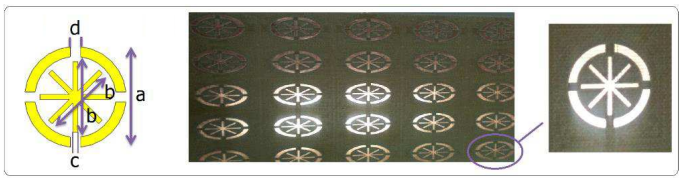

Figure 1. Proposed dual-band MA. (a) Dimensions of the unit cell. (b) A picture of the sample.

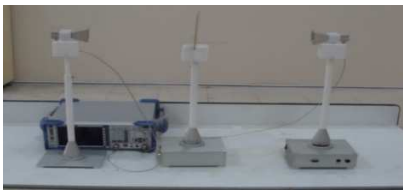

Figure 2. A picture from the measurement.

3. RESULTS AND ANALYSIS

The numerical and experimental results are compared and verified to show the proposed absorber performance. The experimental results show good agreement with the simulation results. Simulated and measured reflection and absorption results are presented in Fig. 3 and Fig. 4, respectively. It can be seen from the simulation that maximum absorption of 95.6% and 99.9% is observed at 4.32 GHz and 5.73 GHz, in order. The corresponding reflection values are 0.21 and 0.02 at the first (4.32 GHz) and second (5.73 GHz) resonances. Two maxima in the absorption are experimentally obtained around

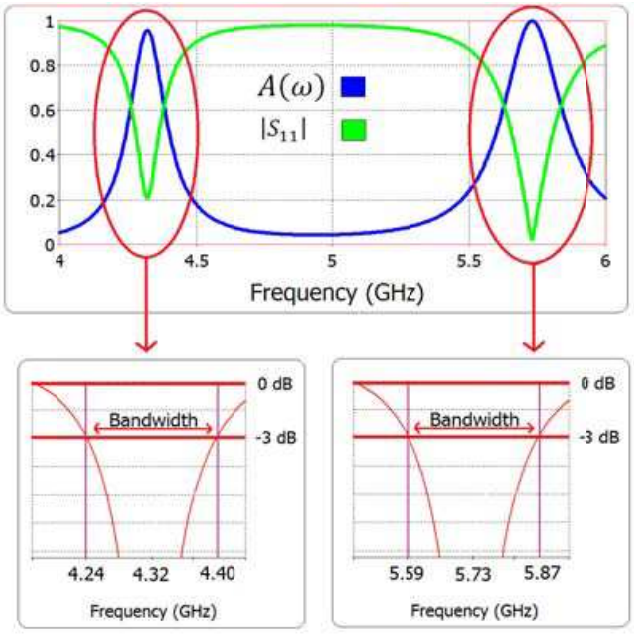

Figure 3. Simulated reflection and absorption of the proposed dual-band MA.

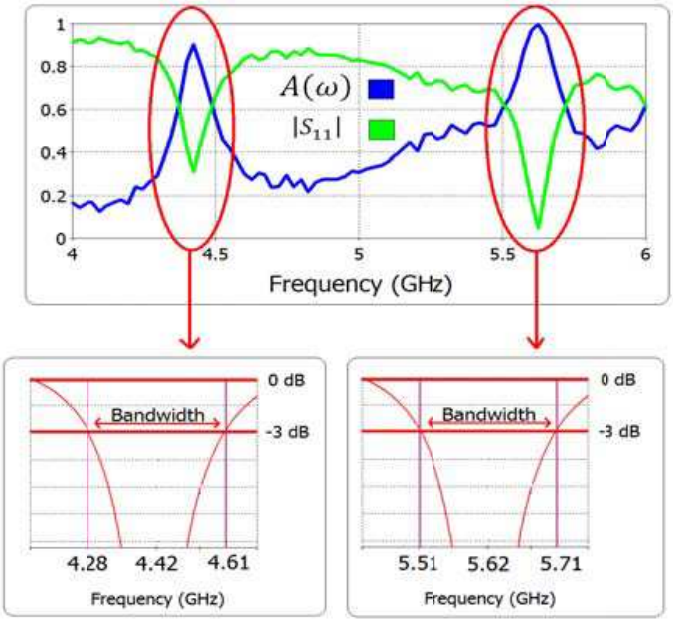

Figure 4. Measured reflection and absorption of the proposed dual-band MA.

90% at 4.42 GHz for the first band and 99.7% at 5.62 GHz for the second band. It can be seen that the proposed model exhibits as a dual-band absorber in which the second absorption is perfect. Note that, the discrepancies between the experimental and simulation data are imputed to fabrication tolerances and dielectric dispersion of the substrate. The misalignment during the experiment may also be considered as another source of error. Additionally, it must be pointed out that the measurement has been performed using only one single slab and that, despite the relatively-small-sized sample used, the resonance effect at the predicted frequency and the data agreement are quite remarkable. Furthermore, only one unit cell was considered with the periodic boundaries in the simulation and the tested small-sized-slab may give life to inconsistencies arising from the interactions among unit cells. This is because of the wave scattering due to small-sized sample. Moreover, the raw measurement data without removing any noise information (also without any correction, fitting, smoothing, filtering, etc.) are presented in Fig. 4. The accuracy of the measurements can be clarified by the good agreement between the simulation and experimental results [20]. The absorption magnitude of the two maxima is better than that of the studies in the literature. Whereas two maxima have been observed in the same frequency range in the studies, the absorption magnitudes of the proposed absorber are improved either for the first or second resonance with respect to the absorbers in the literature [15, 29, 41]. Additionally, bandwidth calculations are performed to show the quality of the proposed dual-band MA as can be seen in Fig. 3 and Fig. 4. The bandwidth sometimes plays an important role in many absorber applications such as in communication systems. So that, the fractional bandwidth (FBW) can be calculated as $FBW = \Delta f/f_0$, where Δf is the half-power bandwidth and f_0 is the center frequency. For the proposed model, these parameters are obtained from the simulation as $\Delta f = 0.16\,\text{GHz}$ & $0.28\,\text{GHz}$, $f_0 = 4.32\,\text{GHz}$ & $5.73\,\text{GHz}$ and $FBW \approx 3.70\%\,\text{GHz}$ & 4.88% for first and second resonances. From the experiment, we have the following values: $\Delta f = 0.33\,\text{GHz}$ & $0.20\,\text{GHz}$, $f_0 = 4.42\,\text{GHz}$ & $5.62\,\text{GHz}$ and $FBW \approx 7.46\%$ & 3.55% for first and second resonance modes, in order. These calculations signify that the proposed model has good quality with respect to bandwidth.

In order to monitor the absorbing performance of the proposed structure, the effects of the horizontal and vertical gaps are investigated for the sake of comparison. This is beneficial to deeper understanding the operating mechanism of the absorber when they are combined. The results are shown in Fig. 5. For the studied spectrum, two different configurations have one resonance. As a first configuration (horizontal gaps, red one), the vertical gaps are closed. The structure provides a resonance with $S_{11} = 0.093$ at the frequency of 5.54 GHz. Absorption value is 99.13%. Furthermore, as a second configuration (vertical gaps, green one), the horizontal gaps are closed. The structure shows a resonance with $S_{11} = 0.16$ at the frequency of 2.94 GHz. Absorption value is 97.44%. This means that the combined structure can provide two absorption bands at two distinct frequencies. The relative reduction in the first band in the combined structure (see Fig. 3 and Fig. 5) with respect to the corresponding individual structure can be explained as contradictory interaction of the fields localized at the gaps which will be explained in the following sections. This reduction can/may be minimized (or made negligible) by the optimization of the dimensions of the structure.

Another investigation for understanding the operation mechanism for the individual horizontal and vertical gaps is the electric field, magnetic field, and surface current distribution which can be seen in Fig. 6. From the field distribution, one can claim that the resonance modes are different than each

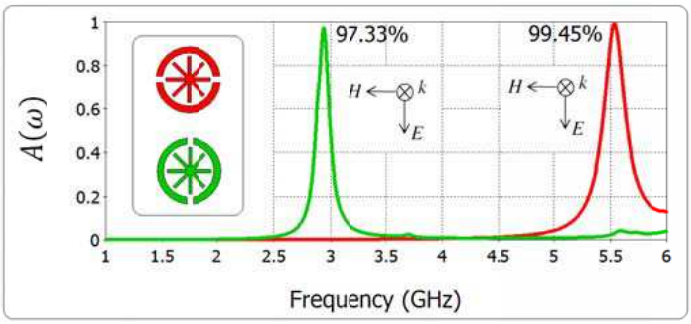

Figure 5. Simulated absorptivity of the modified MA.

other. In addition, the horizontal gaps are responsible from the electrical resonance and the vertical ones are from the magnetic resonance. The dominant mode forms the character of the resonances. This can be seen from the surface current distribution as well. Symmetric currents create the electrical resonance while the circulating and anti-symmetric currents create the magnetic one. These symmetric, anti-symmetric, and circulating currents result in electric and magnetic resonances which strongly match with the incident electromagnetic wave. The observed electric and magnetic resonances provide nearly-complete impedance matching between the MA and air ($Z(\omega) = Z_0(\omega)$). In other words, complete absorption a phenomenon is achieved due to the restrained EM energy [41].

In order to understand the physical mechanism of the operation principle of proposed dual-band MA at the resonances, the electric field and surface current distributions are presented in Figs. 7–10. The electric field and surface current distributions are separately obtained and evaluated for the absorber at the resonant frequencies of 4.32 GHz and 5.73 GHz. Fig. 7 and Fig. 8 show the electric field distributions for first and second resonance frequencies of 4.32 GHz and 5.73 GHz, respectively. It can be seen that while the first resonance provides high concentration of electric field around the corner of OSS (except the horizontal strip), the second resonance provides higher concentration of electric field around gaps of the ring. This means each mode has different character as mentioned in the previous paragraph. In the first resonance of 4.32 GHz, the electric field is localized at the upper and lower half planes with respect to the horizontal strip. Hence the structure behaves as an electrical dipole for the applied polarization. For the second resonance, high localization of the electric field around gaps is observed. Note that, this mode is better than the first one in the combined structure and provides better absorption with respect to the first resonance (99.9%). This may attributed to the positive coupling of the fields in the combined structure.

Also, Fig. 9 and Fig. 10 show the surface current distributions for first and second resonance frequencies of 4.32 GHz and 5.73 GHz, respectively. It can be seen that they have different distribution

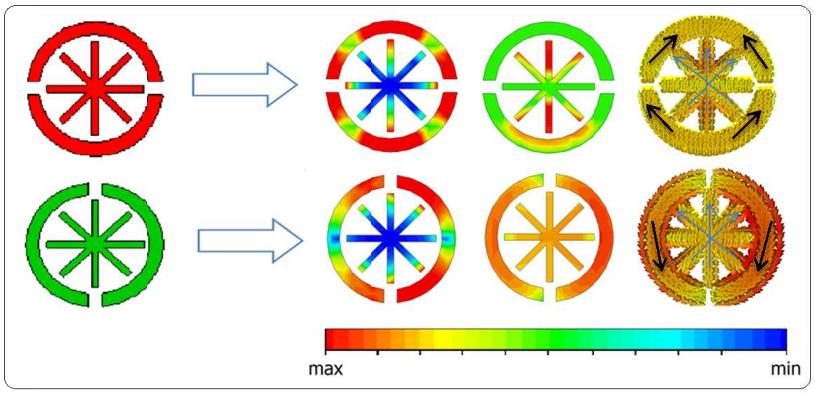

Figure 6. Simulated electric field, magnetic field, and surface current for the individual horizontal and vertical gaps.

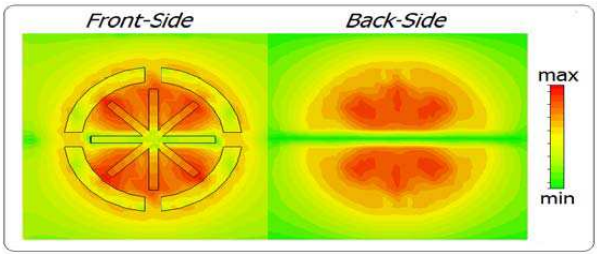

Figure 7. Electric field distribution at the first resonance frequency of 4.32 GHz.

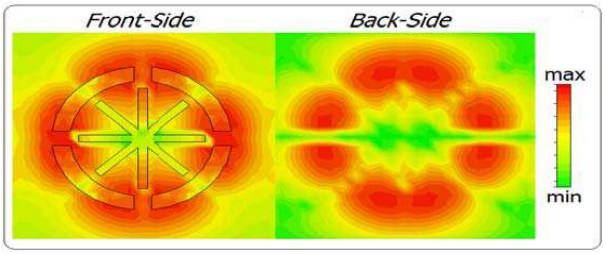

Figure 8. Electric field distribution at the second resonance frequency of 5.73 GHz.

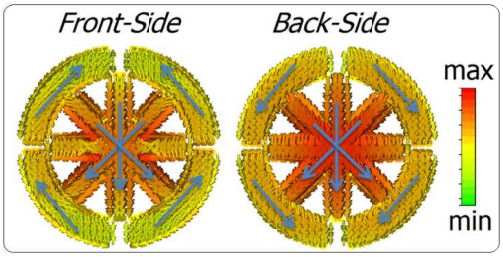

Figure 9. Surface current distribution at the first resonance frequency of 4.32 GHz.

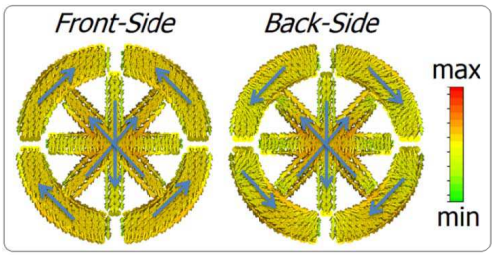

Figure 10. Surface current distribution at the second resonance frequency of 5.73 GHz.

which clarifies the different character of the resonances. High concentration of the currents along the strips at the first resonance holds a signature of the domination of the electric resonance. The polarization of the strips creates surface charges and current circulation. The current circulation excites magnetic response and as a result an absorption phenomenon rises. The current distribution includes the circulating, symmetric, and anti-symmetric currents (Fig. 9). The currents are denser along the strips than the ring. While the strong symmetric currents along the strips are due to the electrical response, weaker anti-parallel currents along the ring results from the magnetic effects. The similar remarks can also be observed for the second resonance mode. The electric and magnetic responses of the overall system matches with the electric and magnetic components of the incident wave. These resonances provide absorption of the EM wave at the resonance frequency with good impedance matching. Therefore, the incident wave is restrained in the MA which results in a minimization of the reflection and maximization of the absorption. The current pattern of the second mode is similar to the first resonance and its intensity is more proportional. The structure creates both the electric and magnetic resonances similar to the previous one with the additional field coupling. Therefore, the second absorption mode is better than the first mode [41].

Furthermore, the effects of incident and polarization angle on the characteristic of the dual-band MA are observed. The incident angle is rotated from 0° to 90° with 15° steps. Fig. 11 shows absorption performance of the proposed dual-band MA model for different incident angles. It can be seen that the proposed model provides very well absorption for all incident angles. When the incident angle is changed, only very small differences occurs. This shows that the proposed MA perfectly provides incident angle independency. This can be attributed as an added value to the performance of the proposed MA.

Moreover in this sense, Fig. 12 shows the simulated absorption dependency as a function of frequency between 0° and 90° polarization angles for the transverse electric (TE) and the transverse magnetic (TM) polarized waves. The absorption values are shown in Table 1. The first mode and the second mode are approximately located at around 5.10 GHz and 6.23 GHz, respectively. The frequency shift can be explained by the change of the polarization state. As seen, there are very small and negligible differences between the cases of TE and TM when the polarization angle is changed since the proposed model is flexible and multi directional structure. The important issue is that the first mode for some polarization angles and polarization type is greatly enhanced. The simulated results show that the dual-band MA can be operated for a wide range of incident angle and arbitrary polarization.

4. DISCUSSION

As seen from the simulation and experimental results, the proposed dual-band MA shows perfect absorber properties for the studied frequency region with the insensitivity of the polarization and incident angles. Unlike the proposed structure, many studies in literature show only insensitivity for the polarization and incident angle only for limited angles. This is one of the advantages of the proposed absorber based on its isotropic features. Furthermore, MA presented here has simpler configuration than some of its counterparts. Moreover, its symmetric configuration can be attributed as another source of advantage since it is directly related with the spatial features (bianisotropic, anisotropic, biisotropic, or isotropic) of the structure. In this sense, it is worth to investigate the frequency response of the

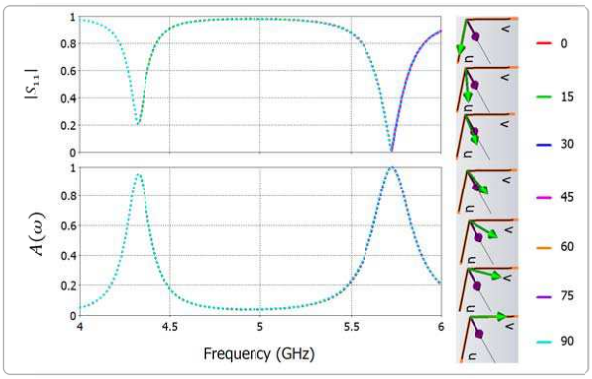

Figure 11. Simulated reflection and absorption characteristics at different incident angles.

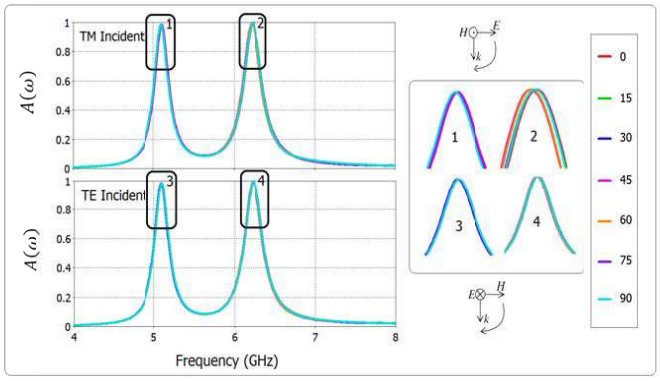

Figure 12. Simulated angular dependency of the absorption properties for TE and TM waves.

Table 1. Simulated absorption values at the resonances for TE and TM waves.

Angle (degrees)	***TE* Wave**		***TM* Wave**	
	First	Second	First	Second
0°	98.46%	99.91%	98.46%	99.89%
15°	98.49%	99.81%	98.58%	99.88%
30°	98.56%	99.93%	98.52%	99.65%
45°	98.51%	99.96%	98.50%	99.93%
60°	98.45%	99.97%	98.53%	99.94%
75°	98.47%	99.72%	98.56%	99.90%
90°	98.37%	99.91%	98.41%	99.94%

chirality (degree of the isotropy) [42] for the proposed resonator and compare it with its counterpart(s) existing literature. Thus, the chirality for the proposed resonator and for Ref. [41] (Ω resonator with gap and OSS) are obtained [42] and the result is shown in Fig. 13. As seen from the figure, the proposed resonator has no chirality while the structure given in Ref. [41] has frequency dependent chirality. This means that the former (the proposed one of this study) is isotropic whereas the latter (Ref. [41]) is not isotropic. The latter can be regarded as biisotropic or chiral structure in which electric and magnetic polarizations can be induced by both electric and magnetic fields since there is a coupling between them. This coupling is determined by the degree (strength) of chirality. Therefore, both structures are abundant and useful depending on the requirement/demand and they can be used where isotropy and biisotropy (this study and Ref. [41], respectively) is needed. Although the structure given in Ref. [41] also provides polarization and incident angle independencies, the proposed structure of this study is much sensitive to the polarization and incident angle variations. The frequency response of the proposed one (Fig. 11 and Fig. 12) is more clean, pure, and smooth (with respect to isotropy) while the structure of Ref. [41] is not (Fig. 9 and Fig. 10 of Ref. [41]). The additional peaks appears in Fig. 9 and Fig. 10 of Ref. [41] come from the biisotropic property (electric and magnetic fields coupling) of the structure and sometimes these peaks are unwanted depending on the application(s). Thus, the proposed MA is has better performance and very efficient than non-isotropic MTM-based absorbers when the polarization and incident angle are very critical in the designated application. Consequently, considering the results of the both structures, one can conclude that it is possible to achieve perfect absorption for both isotropic and non-isotropic structures with different physical features. Superiority of one over the other is changed according to the application. Note that the comments given for the proposed MA are based on the superiority of the isotropy.

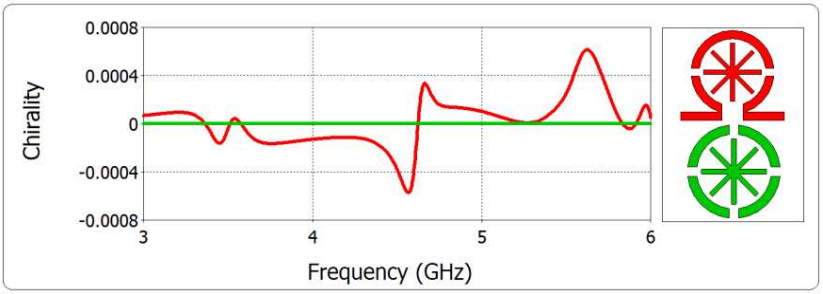

Figure 13. Simulations results of the chirality parameter for proposed model and Ref. [41].

Besides, the results show that it is possible to adjust the number of absorption bands with polarization and incident angle independencies by proper selection of the structural configuration. For example, the structural symmetric configurations with variable dimensions in one unit cell can be chosen to realize multi-absorption bands with polarization and incident angle independencies as well as without additional (unwanted) peaks (clean, pure, and smooth absorption peaks as in the present study). In addition, the mechanism can be adopted for other regime of electromagnetic spectrum such as millimeter-wave, THz, and so on. Hence, it can be concluded that the suggested model has many advantages such as simplicity, flexibility, dual-band, solid insensitivity for all polarizations and incident angles; and can be used to realize myriad MTM based absorbers.

5. CONCLUSION

Dual-band polarization and incident angle independent MA is numerically and experimentally examined, and the obtained results are confirmed by the comparison of the simulated and measured data with good agreement. According to the results, the investigated MA provides perfect and dual-band absorption at resonance frequencies independent from the polarization state and incident angles. At some cases of the polarization states and incident angles, the absorption value can be enhanced. The isotropic feature of the proposed MA is also discussed and compared with literature in which the isotropic property of the structure (additional positive advantage) can also be used in several applications where the isotropic absorbers are needed. The verified polarization and incident angle independent MA can be used as a dual-band absorber and can be a good candidate for the applications of stealth, sensor, medical imaging, and so on.

REFERENCES

1. Vesalago, V. G., "The electrodynamics of substances with simultaneously negative values of ε and μ," *Sov. Phys. Usp.*, Vol. 10, No. 4, 509–514, 1968.
2. Shelby, R. A., D. Smith, and S. Schultz, "Experimental verification of a negative index of refraction," *Science*, Vol. 292, No. 5514, 77–79, 2001.
3. Chen, X., "Implicit boundary conditions in transformation-optics cloaking for electromagnetic waves," *Progress In Electromagnetics Research*, Vol. 121, 521–534, 2011.
4. Silva-Macêdo, J. A., M. A. Romero, and B.-H. V. Borges, "An extended FDTD method for the analysis of electromagnetic field rotators and cloaking devices," *Progress In Electromagnetics Research*, Vol. 87, 183–196, 2008.
5. Zhang, Y. and M. A. Fiddy, "Covered image of superlens," *Progress In Electromagnetics Research*, Vol. 136, 225–238, 2013.
6. Cai, M. and E. P. Li, "A novel terahertz sensing device comprising of a parabolic reflective surface and a bi-conical structure," *Progress In Electromagnetics Research*, Vol. 97, 61–73, 2009.
7. Bilotti, F., L. Nucci, and L. Vegni, "An SRR-based microwave absorber," *Microw. Opt. Techn. Let.*, Vol. 48, 2171–2175, 2006.

8. Landy, N. I., S. Sajuyigbe, J. J. Mock, D. R. Smith, and W. J. Padilla, "A perfect metamaterial absorber," *Phys. Rev. Lett.*, Vol. 100, 207402-4, 2008.
9. Lee, J. and S. Lim, "Bandwidth-enhanced and polarization-insensitive metamaterial absorber using double resonance," *Electron. Lett.*, Vol. 47, No. 1, 8–9, 2011.
10. Sun, J., L. Liu, G. Dong, and J. Zhou, "An extremely broad band metamaterial absorber based on destructive interference," *Opt. Express*, Vol. 19, No. 22, 21155–21162, 2011.
11. Li, L., Y. Yang, and C. H. Liang, "A wide-angle polarization-insensitive ultra-thin metamaterial absorber with three resonant modes," *J. Appl. Phys.*, Vol. 110, 063702, 2011.
12. Park, J. W., P. V. Tuong, J. Y. Rhee, K. W. Kim, W. H. Jang, E. H. Choi, L. Y. Chen, and Y. Lee, "Multi-band metamaterial absorber based on the arrangement of donut-type resonators," *Opt. Express*, Vol. 21, No. 8, 9691–9702, 2013.
13. Wang, B., T. Koschny, and C. M. Soukoulis, "Wide-angle and polarization-independent chiral metamaterial absorber," *Phys. Rev. B*, Vol. 80, 033108-4, 2009.
14. Zhu, B., Y. Feng, J. Zhao, C. Huang, Z. Wang, and T. Jiang, "Polarization modulation by tunable electromagnetic metamaterial reflector/absorber," *Opt. Express*, Vol. 18, No. 22, 23196–23203, 2010.
15. Zhu, B., Z. Wang, C. Huang, Y. Feng, J. Zhao, and T. Jiang, "Polarization insensitive metamaterial absorber with wide incident angle," *Progress In Electromagnetics Research*, Vol. 101, 231–239, 2010.
16. Huang, Y. J., G. J. Wen, J. Li, W. R. Zhu, P. Wang, and Y. H. Sun, "Wide-angle and polarization-independent metamaterial absorber based on snowflake-shaped configuration," *Journal of Electromagnetic Waves and Applications*, Vol. 27, No. 5, 552–559, 2013.
17. Sabah, C. and S. Uckun, "Multilayer system of Lorentz/Drude type metamaterials with dielectric slabs and its application to electromagnetic filters," *Progress In Electromagnetics Research*, Vol. 91, 349–364, 2009.
18. Sabah, C., H. T. Tastan, F. Dincer, K. Delihacioglu, M. Karaaslan, and E. Unal, "Transmission tunneling through the multi-layer double-negative and double-positive slabs," *Progress In Electromagnetics Research*, Vol. 138, 293–306, 2013.
19. Sabah, C. and H. G. Roskos, "Design of a terahertz polarization rotator based on a periodic sequence of chiral metamaterial and dielectric slabs," *Progress In Electromagnetics Research*, Vol. 124, 301–314, 2012.
20. Sabah, C. and F. Urbani, "Experimental analysis of Λ-shaped magnetic resonator for mu-negative metamaterials," *Opt. Commun.*, Vol. 294, 409–413, 2013.
21. Wiltshire, M. C. K., J. B. Pendry, I. R. Young, D. J. Larkman, D. J. Gilderdale, and J. V. Hajnal, "Microstructured magnetic materials for RF flux guides in magnetic resonance imaging," *Science*, Vol. 291, No. 5505, 849–851, 2001.
22. Sabah, C. and H. G. Roskos, "Terahertz sensing application by using planar split-ring-resonator structures," *Microsyst. Technol.*, Vol. 18, 2071–2076, 2012.
23. Sabah, C., "Multi-resonant metamaterial design based on concentric V-shaped magnetic resonators," *Journal of Electromagnetic Waves and Applications*, Vol. 26, Nos. 8–9, 1105–1115, 2012.
24. Sabah, C., "Electric and magnetic excitations in anisotropic broadside-coupled triangular-split-ring resonators," *Appl. Phys. A: Mater. Sci. Process.*, Vol. 108, 457–463, 2012.
25. Sabah, C., "Microwave response of octagon-shaped parallel plates: Low-loss metamaterial," *Opt. Commun.*, Vol. 285, Nos. 21–22, 4549–4552, 2012.
26. Sabah, C. and H. G. Roskos, "Broadside-coupled triangular split-ring-resonators for terahertz sensing," *Eur. Phys. J. — Appl. Phys.*, Vol. 61, 30402, 2013.
27. Sabah, C., "Multiband metamaterials based on multiple concentric open-ring resonators topology," *IEEE J. Sel. Top. Quant. Electron.*, Vol. 19, 8500808, 2013.
28. Dincer, F., C. Sabah, M. Karaaslan, E. Unal, M. Bakir, and U. Erdiven, "Asymmetric transmission of linearly polarized waves and dynamically wave rotation using chiral metamaterial," *Progress In Electromagnetics Research*, Vol.140, 227–239, 2013.

29. Huang, L. and H. Chen, "Multi-band and polarization insensitive metamaterial absorber," *Progress In Electromagnetics Research*, Vol. 113, 103–110, 2011.
30. Iqbal, M. N., M. F. B. A. Malek, S. H. Ronald, M. S. Bin Mezan, K. M. Juni, and R. Chat, "A study of the EMC performance of a graded-impedance, microwave, rice-husk absorber," *Progress In Electromagnetics Research*, Vol. 131, 19–44, 2012.
31. Faruque, M. R. I., M. T. Islam, and N. Misran, "Design analysis of new metamaterial for EM absorption reduction," *Progress In Electromagnetics Research*, Vol. 124, 119–135, 2012.
32. Gong, Y., K. Li, J. Huang, N. J. Copner, A. Davies, L. Wang, and T. Duan, "Frequency-selective nanostructured plasmonic absorber by highly lossy interface mode," *Progress In Electromagnetics Research*, Vol. 124, 511–525, 2012.
33. Chung, B.-K. and H.-T. Chuah, "Modeling of RF absorber for application in the design of anechoic chamber," *Progress In Electromagnetics Research*, Vol. 43, 273–285, 2003.
34. Chamaani, S., S. A. Mirtaheri, M. Teshnehlab, M. A. Shooredeli, and V. Seydi, "Modified multi-objective particle swarm optimization for electromagnetic absorber design," *Progress In Electromagnetics Research*, Vol. 79, 353–366, 2008.
35. Malek, M. F. B. A., E. M. Cheng, O. Nadiah, H. Nornikman, M. Ahmed, M. Z. A. Abdul Aziz, A. R. Othman, P. J. Soh, A. A. A.-H. Azremi, A. Hasnain, and M. N. Taib, "Rubber tire dust-rice husk pyramidal microwave absorber," *Progress In Electromagnetics Research*, Vol. 117, 449–477, 2011.
36. Nornikman, H., B. H. Ahmad, M. Z. A. Abdul Aziz, M. F. B. A. Malek, H. Imran, and A. R. Othman, "Study and simulation of an edge couple split ring resonator (EC-SRR) on truncated pyramidal microwave absorber," *Progress In Electromagnetics Research*, Vol. 127, 319–334, 2012.
37. Ramprecht, J., M. Norgren, and D. Sjoberg, "Scattering from a thin magnetic layer with a periodic lateral magnetization: Application to electromagnetic absorbers," *Progress In Electromagnetics Research*, Vol. 83, 199–224, 2008.
38. Klemm, M. and G. Troester, "EM energy absorption in the human body tissues due to UWB antennas," *Progress In Electromagnetics Research*, Vol. 62, 261–280, 2006.
39. Li, M., H.-L. Yang, X.-W. Hou, Y. Tian, and D.-Y. Hou, "Perfect metamaterial absorber with dual bands," *Progress In Electromagnetics Research*, Vol. 108, 37–49, 2010.
40. He, X.-J., Y. Wang, J. Wang, T. Gui, and Q. Wu, "Dual-band terahertz metamaterial absorber with polarization insensitivity and wide incident angle," *Progress In Electromagnetics Research*, Vol. 115, 381–397, 2011.
41. Dincer, F., M. Karaaslan, E. Unal, and C. Sabah, "Dual-band polarization independent metamaterial absorber based on omega resoanator and octa-star strip configuration," *Progress In Electromagnetics Research*, Vol. 141, 219–231, 2013.
42. Dincer, F., C. Sabah, M. Karaaslan, E. Unal, M. Bakir, and U. Erdiven, "Asymmetric transmission of linearly polarized waves and dynamically wave rotation using chiral metamaterial," *Progress In Electromagnetics Research*, Vol. 140, 227–239, 2013.